Available online at www.sciencedirect.com
SCIENCE DIRECT®
International Journal of Engineering Science 43 (2005) 321–339
International Journal of Engineering Science
www.elsevier.com/locate/ijengsci

Exact solution for functionally graded and layered magneto-electro-elastic plates

E. Pan *, F. Han

Department of Civil Engineering, ASEC, University of Akron, Akron, OH 44325-3905, United States

Received 22 August 2003; received in revised form 23 November 2003; accepted 23 November 2004

Abstract

In this paper, an exact solution is presented for the multilayered rectangular plate made of functionally graded, anisotropic, and linear magneto-electro-elastic materials. While the edges of the plate are under simply supported conditions, general mechanical, electric and magnetic boundary conditions can be applied on both the top and bottom surfaces of the plate. The functionally graded material is assumed to be exponential in the thickness direction and the homogeneous solution in each layer is obtained based on the pseudo-Stroh formalism. For multilayered plate structure, the propagator matrix method is employed so that only a 5×5 system of linear algebraic equations needs to be solved. The exact solution is then applied to two functionally graded (exponential) sandwich plates made of piezoelectric $BaTiO_3$ and magnetostrictive $CoFe_2O_4$, under mechanical and electric loads on the top surface. While the numerical results clearly show the influence of the exponential factor, magneto-electro-elastic properties, and loading types on induced magneto-electric-elastic fields, they can also serve as benchmarks to numerical methods such as the finite and boundary element methods.

Keywords: Functionally graded material; Magneto-electro-elastic plate; Propagator matrix; Pseudo-Stroh formalism

* Corresponding author. Tel.: +1 330 972 6739; fax: +1 330 972 6020.
E-mail address: pan2@uakron.edu (E. Pan).

0020-7225/$ - see front matter © 2005 Elsevier Ltd. All rights reserved.
doi:10.1016/j.ijengsci.2004.09.006

1. Introduction

Smart or intelligent materials such as the piezoelectric and piezomagnetic ones are currently intensively investigated, due to their ability of converting energy from one form to the other (among magnetic, electric and mechanical energies). It is also observed that, composites made of piezoelectric/piezomagnetic materials can exhibit the magnetoelectric coupling that is not present in the single-phase piezoelectric or piezomagnetic material [1–3]. Recently, Pan [4] derived an exact closed-form solution for the simply supported and multilayered plate made of anisotropic piezoelectric and piezomagnetic materials under a static mechanical load, and Pan and Heyliger [5] solved the corresponding vibration problem. On the other hand, Li and Dunn [6] carried out a study on the micromechanics of magneto-electro-elastic composite materials. More recently, Wang and Shen [7] studied the two-dimensional (2D) inclusion problem in magneto-electro-elastic composite materials, and Gao et al. [8] solved the crack problem in 2D magneto-electro-elastic solids.

The functionally graded material (FGM) structure has attracted wide and increasing attentions to scientists and engineers. FGM plays an essential role in most advanced integrated systems for vibration control and health monitoring. While He et al. [9] investigated the FGM plates with integrated piezoelectric sensors and actuators for the active control purpose, Liew et al. [10] analyzed the post buckling of piezoelectric FGM plates subjected to thermo-electro-mechanical loading. The time-dependent stress analysis in FGM elastic cylinders was carried out by Yang [11], and the effect of the inter-diffusion reaction on the compatibility in PZT/PNN FGM materials was analyzed by Xu et al. [12]. Almajid and Taya [13] and Almajid et al. [14] also investigated the displacement and stress fields in piezocomposite plates with functionally graded microstructure for potential applications in the piezoelectric bimorph. More recently, a three-dimensional (3D) exact closed-form solution was derived for anisotropic elastic [15] and piezoelectric [16] FGM plates under simply supported edge conditions.

In this paper, we present an exact solution for a multilayered rectangular plate made of anisotropic and functionally graded magneto-electro-elastic materials. The plate is simply supported along its edges, and both mechanical and electric loads are applied on the top surface. The homogeneous solution is obtained based on the pseudo-Stroh formalism [17–19], and the propagator matrix method [20,21] is employed to treat the multilayered case. In the numerical analysis, two functionally graded (exponential) sandwich plates made of piezoelectric $BaTiO_3$ and magnetostrictive $CoFe_2O_4$ are analyzed. Numerical results clearly show the influence of the exponential factor, magneto-electro-elastic properties, stacking sequence, and loading types on the induced magneto-electric-elastic fields, which should be of interest to the design of smart structures. Furthermore, these numerical examples could also serve as benchmarks to numerical methods such as the finite and boundary element methods.

2. Problem statement and basic formulations

Let us assume that there is an N-layered rectangular plate made of anisotropic and functionally graded magneto-electro-elastic materials and that its four sides are simply supported. The dimensions of the layered plate are $L_x \times L_y \times H$ with H being the thickness. Each layer can be homo-

geneous or functionally graded with exponentially varying material properties. A Cartesian coordinate system is attached to the plate with its origin being at one of the four corners on the bottom; the plate is in the positive z-region. Layer j is bounded by its lower interface (or surface) at $z = z_j$ and upper interface (or surface) at $z = z_{j+1}$ with its thickness $h_j = z_{j+1} - z_j$. Obviously, the bottom surface is at $z = z_1$ (=0) and the top surface at $z = z_{N+1}$ (=H). Without loss of generality, external loads (mechanical, electric or magnetic) will be applied on the top surface of the N-layered plate.

For an anisotropic and linearly magneto-electro-elastic material, the coupled constitutive equations for each layer can be written as

$$\begin{aligned} \sigma_i &= C_{ik}\gamma_k - e_{ki}E_k - q_{ki}H_k \\ D_i &= e_{ik}\gamma_k + \varepsilon_{ik}E_k + d_{ik}H_k \\ B_i &= q_{ik}\gamma_k + d_{ik}E_k + \mu_{ik}H_k \end{aligned} \tag{1}$$

where σ_i, D_i and B_i are the stress, electric displacement and magnetic induction (i.e., magnetic flux), respectively; γ_i, E_i and H_i are the strain, electric field and magnetic field, respectively; C_{ij}, ε_{ij} and μ_{ij} are the elastic, dielectric and magnetic permeability coefficients, respectively; e_{ij}, q_{ij} and d_{ij} are the piezoelectric, piezomagnetic and magnetoelectric coefficients, respectively. Apparently, various uncoupled cases can be reduced from Eq. (1) by setting the appropriate coupling coefficients to zero.

For a functionally graded material with exponential variation in the z-direction, the material coefficients in Eq. (1) can be described by

$$\begin{aligned} &C_{ik}(z) = C^0_{ik}\mathrm{e}^{\eta z}; \quad \varepsilon_{ik}(z) = \varepsilon^0_{ik}\mathrm{e}^{\eta z}; \quad \mu_{ik}(z) = \mu^0_{ik}\mathrm{e}^{\eta z} \\ &e_{ik}(z) = e^0_{ik}\mathrm{e}^{\eta z}; \quad q_{ik}(z) = q^0_{ik}\mathrm{e}^{\eta z}; \quad d_{ik}(z) = d^0_{ik}\mathrm{e}^{\eta z} \end{aligned} \tag{2}$$

where η is the exponential factor characterizing the degree of the material gradient in the z-direction, and the superscript 0 is attached to indicate the z-independent factors in the material coefficients. It is obvious that $\eta = 0$ corresponds to the homogeneous material case.

For an orthotropic solid, with transverse isotropy being a special case, the material coefficients in Eq. (1) can be written as

$$[C] = \begin{bmatrix} C_{11} & C_{12} & C_{13} & 0 & 0 & 0 \\ & C_{22} & C_{23} & 0 & 0 & 0 \\ & & C_{33} & 0 & 0 & 0 \\ & & & C_{44} & 0 & 0 \\ & \mathit{Sym} & & & C_{55} & 0 \\ & & & & & C_{66} \end{bmatrix}, \quad [e] = \begin{bmatrix} 0 & 0 & e_{31} \\ 0 & 0 & e_{32} \\ 0 & 0 & e_{33} \\ 0 & e_{24} & 0 \\ e_{15} & 0 & 0 \\ 0 & 0 & 0 \end{bmatrix}, \quad [q] = \begin{bmatrix} 0 & 0 & q_{31} \\ 0 & 0 & q_{32} \\ 0 & 0 & q_{33} \\ 0 & q_{24} & 0 \\ q_{15} & 0 & 0 \\ 0 & 0 & 0 \end{bmatrix} \tag{3}$$

$$[\varepsilon] = \begin{bmatrix} \varepsilon_{11} & 0 & 0 \\ 0 & \varepsilon_{22} & 0 \\ 0 & 0 & \varepsilon_{33} \end{bmatrix}, \quad [d] = \begin{bmatrix} d_{11} & 0 & 0 \\ 0 & d_{22} & 0 \\ 0 & 0 & d_{33} \end{bmatrix}, \quad [\mu] = \begin{bmatrix} \mu_{11} & 0 & 0 \\ 0 & \mu_{22} & 0 \\ 0 & 0 & \mu_{33} \end{bmatrix} \tag{4}$$

The extended strain (using tensor symbol for the elastic strain γ_{ik})–displacement relation is

$$\begin{aligned} \gamma_{ij} &= 0.5(u_{i,j} + u_{j,i}) \\ E_i &= -\phi_{,i}, \quad H_i = -\psi_{,i} \end{aligned} \tag{5}$$

where u_i, ϕ and ψ are, respectively, the elastic displacement, electric potential, and magnetic potential.

The equations of equilibrium, including the balance of the body force and electric charge and current, can be written as:

$$\begin{aligned} \sigma_{ij,j} + f_i &= 0 \\ D_{j,j} - f_e &= 0 \\ B_{j,j} - f_m &= 0 \end{aligned} \tag{6}$$

where f_i, f_e, and f_m are, respectively, the body force, electric charge density, and electric current density (or magnetic charge density as compared to the electric charge density).

3. Stroh-type general solutions

For a simply supported and FGM plate, we seek the solution of the extended displacement vector $\boldsymbol{u}$ in the form [4]

$$\boldsymbol{u} \equiv \begin{bmatrix} u_x \\ u_y \\ u_z \\ \phi \\ \psi \end{bmatrix} = \mathrm{e}^{sz} \begin{bmatrix} a_1 \cos px \sin qy \\ a_2 \sin px \cos qy \\ a_3 \sin px \sin qy \\ a_4 \sin px \sin qy \\ a_5 \sin px \sin qy \end{bmatrix} \tag{7}$$

where

$$p = n\pi/L_x, \quad q = m\pi/L_y \tag{8}$$

with n and m being two positive integers.

It is noted that solution (7) represents only one of the terms in a double Fourier series expansion when solving a general boundary value problem. Therefore, in general, summations for n and m over suitable ranges are implied whenever the sinusoidal term appears.

Substitution of Eq. (7) into the general strain–displacement relations (5), the constitutive equations (1), and finally into the equations of equilibrium (6) with zero force and densities, yields the following eigenequation

$$[\boldsymbol{Q} - \eta \boldsymbol{R}^{\mathrm{t}} + s(\boldsymbol{R} - \boldsymbol{R}^{\mathrm{t}} + \eta \boldsymbol{T}) + s^2 \boldsymbol{T}]\boldsymbol{a} = 0 \tag{9}$$

where superscript t denotes the transpose of the matrix. Also in Eq. (9),

$$\boldsymbol{a} = [a_1, a_2, a_3, a_4, a_5]^{\mathrm{t}} \tag{10}$$

$$\boldsymbol{R}=\begin{bmatrix} 0 & 0 & pC_{13}^0 & pe_{31}^0 & pq_{31}^0 \\ 0 & 0 & qC_{23}^0 & qe_{32}^0 & pq_{32}^0 \\ -pC_{55}^0 & -qC_{44}^0 & 0 & 0 & 0 \\ -pe_{15}^0 & -qe_{24}^0 & 0 & 0 & 0 \\ -pq_{15}^0 & -qq_{24}^0 & 0 & 0 & 0 \end{bmatrix},\quad \boldsymbol{T}=\begin{bmatrix} C_{55}^0 & 0 & 0 & 0 & 0 \\ & C_{44}^0 & 0 & 0 & 0 \\ & & C_{33}^0 & e_{33}^0 & q_{33}^0 \\ & Sym & & -\varepsilon_{33}^0 & -d_{33}^0 \\ & & & & -\mu_{33}^0 \end{bmatrix} \tag{11}$$

$$\boldsymbol{Q}=\begin{bmatrix} -(C_{11}^0p^2+C_{66}^0q^2) & -pq(C_{12}^0+C_{66}^0) & 0 & 0 & 0 \\ & -(C_{66}^0p^2+C_{22}^0q^2) & 0 & 0 & 0 \\ & & -(C_{55}^0p^2+C_{44}^0q^2) & -(e_{15}^0p^2+e_{24}^0q^2) & -(q_{15}^0p^2+q_{24}^0q^2) \\ & Sym & & \varepsilon_{11}^0p^2+\varepsilon_{22}^0q^2 & d_{11}^0p^2+d_{22}^0q^2 \\ & & & & \mu_{11}^0p^2+\mu_{22}^0q^2 \end{bmatrix} \tag{12}$$

We remark that when the gradient coefficient $\eta = 0$, Eq. (9) is reduced to the eigenequation for the corresponding homogeneous case [4].

We now express the extended traction vector $\boldsymbol{t}$ as

$$\boldsymbol{t}\equiv\begin{bmatrix}\sigma_{xz}\\ \sigma_{yz}\\ \sigma_{zz}\\ D_z\\ B_z\end{bmatrix}=\mathrm{e}^{(s+\eta)z}\begin{bmatrix}b_1\cos px\sin qy\\ b_2\sin px\cos qy\\ b_3\sin px\sin qy\\ b_4\sin px\sin qy\\ b_5\sin px\sin qy\end{bmatrix} \tag{13}$$

which is different from the corresponding homogeneous case [4]. By virtue of the constitutive relations (1) and the displacement expression (7), we obtain

$$\boldsymbol{b}=(-\boldsymbol{R}^{\mathrm{t}}+s\boldsymbol{T})\boldsymbol{a} \tag{14}$$

where

$$\boldsymbol{b}=[b_1,b_2,b_3,b_4,b_5]^{\mathrm{t}} \tag{15}$$

Similarly, the in-plane stresses and electric and magnetic displacements can be expressed as

$$\begin{bmatrix}\sigma_{xx}\\ \sigma_{xy}\\ \sigma_{yy}\\ D_x\\ D_y\\ B_x\\ B_y\end{bmatrix}=\mathrm{e}^{(s+\eta)z}\begin{bmatrix}c_1\sin px\sin qy\\ c_2\cos px\cos qy\\ c_3\sin px\sin qy\\ c_4\cos px\sin qy\\ c_5\sin px\cos qy\\ c_6\cos px\sin qy\\ c_7\sin px\cos qy\end{bmatrix} \tag{16}$$

where

$$\begin{bmatrix} c_1 \\ c_2 \\ c_3 \\ c_4 \\ c_5 \\ c_6 \\ c_7 \end{bmatrix} = \begin{bmatrix} -C^0_{11}p & -C^0_{12}q & C^0_{13}s & e^0_{31}s & q^0_{31}s \\ C^0_{66}q & C^0_{66}p & 0 & 0 & 0 \\ -C^0_{12}p & -C^0_{22}q & C^0_{23}s & e^0_{32}s & q^0_{32}s \\ e^0_{15}s & 0 & e^0_{15}p & -\varepsilon^0_{11}p & -d^0_{11}p \\ 0 & e^0_{24}s & e^0_{24}q & -\varepsilon^0_{22}q & -d^0_{22}q \\ q^0_{15}s & 0 & q^0_{15}p & -d^0_{11}p & -\mu^0_{11}p \\ 0 & q^0_{24}s & q^0_{24}q & -d^0_{22}q & -\mu^0_{22}q \end{bmatrix} \begin{bmatrix} a_1 \\ a_2 \\ a_3 \\ a_4 \\ a_5 \end{bmatrix} \tag{17}$$

These extended stresses (Eq. (13)) should satisfy the equations of equilibrium (assuming zero body force and zero electric and magnetic charge densities).

We remark that Eq. (9), derived for a simply supported plate, resembles the Stroh formalism [17,18]. For the corresponding homogeneous case, this equation was named as pseudo-Stroh formalism because of its similarity to the Stroh formalism [4]. In the present pseudo-Stroh formalism, an interesting feature is observed: That is, if s is a complex (or purely imaginary) eigenvalue, then its complex conjugate is also an eigenvalue.

With aid of Eq. (14), Eq. (9) can now be recast as a 10×10 linear eigensystem

$$\boldsymbol{N}\begin{bmatrix} \boldsymbol{a} \\ \boldsymbol{b} \end{bmatrix} = s\begin{bmatrix} \boldsymbol{a} \\ \boldsymbol{b} \end{bmatrix} \tag{18}$$

where

$$\boldsymbol{N} = \begin{bmatrix} \boldsymbol{T}^{-1}\boldsymbol{R}^{\mathrm{t}} & \boldsymbol{T}^{-1} \\ -\boldsymbol{Q}-\boldsymbol{R}\boldsymbol{T}^{-1}\boldsymbol{R}^{\mathrm{t}} & -\boldsymbol{R}\boldsymbol{T}^{-1}-\eta\boldsymbol{I} \end{bmatrix} \tag{19}$$

Depending upon the given material property, the 10 eigenvalues of Eq. (18) may not be distinct. Should repeated roots occur, a slight change in the material constants would result in distinct roots with negligible error [22] so that for all material situations, the simple and unified solution given below can still be used.

Thus, let us assume that the first five eigenvalues have positive real parts (if the root is purely imaginary, we then pick up the one with positive imaginary part) and the reminders have opposite signs to the first five. We distinguish the corresponding 10 eigenvectors by attaching a subscript to $\boldsymbol{a}$ and $\boldsymbol{b}$. Then the general solution for the extended displacement and traction vectors (of the z-dependent factor) are derived as

$$\begin{bmatrix} \boldsymbol{u} \\ \boldsymbol{t} \end{bmatrix} = \begin{bmatrix} \boldsymbol{A}_1\langle \mathrm{e}^{s^*z}\rangle & \boldsymbol{A}_2\langle \mathrm{e}^{-s^*z}\rangle \\ \boldsymbol{B}_1\langle \mathrm{e}^{(s^*+\eta)z}\rangle & \boldsymbol{B}_2\langle \mathrm{e}^{(-s^*+\eta)z}\rangle \end{bmatrix} \begin{bmatrix} \boldsymbol{K}_1 \\ \boldsymbol{K}_2 \end{bmatrix} \tag{20}$$

where

$$\begin{aligned} &\boldsymbol{A}_1 = [\boldsymbol{a}_1,\boldsymbol{a}_2,\boldsymbol{a}_3,\boldsymbol{a}_4,\boldsymbol{a}_5], \quad \boldsymbol{A}_2 = [\boldsymbol{a}_6,\boldsymbol{a}_7,\boldsymbol{a}_8,\boldsymbol{a}_9,\boldsymbol{a}_{10}] \\ &\boldsymbol{B}_1 = [\boldsymbol{b}_1,\boldsymbol{b}_2,\boldsymbol{b}_3,\boldsymbol{b}_4,\boldsymbol{b}_5], \quad \boldsymbol{B}_2 = [\boldsymbol{b}_6,\boldsymbol{b}_7,\boldsymbol{b}_8,\boldsymbol{b}_9,\boldsymbol{b}_{10}] \\ &\langle \mathrm{e}^{s^*z}\rangle = \mathrm{diag}[\mathrm{e}^{s_1z},\mathrm{e}^{s_2z},\mathrm{e}^{s_3z},\mathrm{e}^{s_4z},\mathrm{e}^{s_5z}] \end{aligned} \tag{21}$$

and $\boldsymbol{K}_1$ and $\boldsymbol{K}_2$ are two 5×1 constant column matrices to be determined.

Eq. (20) is a general solution for a simply supported magneto-electro-elastic FGM plate and reduces to the solution for the corresponding homogeneous plate case. It should be further noticed that new FGM thin plate models could also be reduced from this solution by expanding the exponential term in terms of a Taylor series [23]. This is particularly convenient since one need only to replace the diagonal exponential matrix with its Taylor series expansion [24,25].

With Eq. (20) being served as a general solution for a FGM magneto-electro-elastic plate, solutions for the corresponding multilayered FGM plate can be obtained using the continuity conditions along the interface and the boundary conditions on the top and bottom surfaces of the plate. To handle a multilayered structure with relatively large numbers of layers, we employ the propagator matrix method, instead of the conventional approach [26,27]. The propagator matrix method was developed exclusively for layered structures and possesses certain merits (for a brief review, see [21]), as can be observed in the next section.

4. Solution of multilayered FGM system

From the general solution (20), we solve the column coefficient matrices $\boldsymbol{K}_1$ and $\boldsymbol{K}_2$ for layer j

$$\begin{bmatrix} \boldsymbol{K}_1 \\ \boldsymbol{K}_2 \end{bmatrix}_j = \begin{bmatrix} \boldsymbol{A}_1\langle \mathrm{e}^{s^*(z-z_j)}\rangle & \boldsymbol{A}_2\langle \mathrm{e}^{-s^*(z-z_j)}\rangle \\ \boldsymbol{B}_1\langle \mathrm{e}^{(s^*+\eta)(z-z_j)}\rangle & \boldsymbol{B}_2\langle \mathrm{e}^{(-s^*+\eta)(z-z_j)}\rangle \end{bmatrix}^{-1} \begin{bmatrix} \boldsymbol{u} \\ \boldsymbol{t} \end{bmatrix}_j \tag{22}$$

where the subscript j indicates layer j and s^* are the eigenvalues of layer j.

Let $z = z_j$ and z_{j+1} in Eq. (22), we find that the column coefficient matrices $\boldsymbol{K}_1$ and $\boldsymbol{K}_2$ can be expressed by the displacement $\boldsymbol{u}$ and traction $\boldsymbol{t}$ on either the lower interface or the upper interface of layer j. In other words, we have

$$\begin{bmatrix} \boldsymbol{K}_1 \\ \boldsymbol{K}_2 \end{bmatrix}_j = \begin{bmatrix} \boldsymbol{A}_1 & \boldsymbol{A}_2 \\ \boldsymbol{B}_1 & \boldsymbol{B}_2 \end{bmatrix}_j^{-1} \begin{bmatrix} \boldsymbol{u} \\ \boldsymbol{t} \end{bmatrix}_{z_j} = \begin{bmatrix} \boldsymbol{A}_1\langle \mathrm{e}^{s^*h_j}\rangle & \boldsymbol{A}_2\langle \mathrm{e}^{-s^*h_j}\rangle \\ \boldsymbol{B}_1\langle \mathrm{e}^{(s^*+\eta)h_j}\rangle & \boldsymbol{B}_2\langle \mathrm{e}^{(-s^*+\eta)h_j}\rangle \end{bmatrix}_j^{-1} \begin{bmatrix} \boldsymbol{u} \\ \boldsymbol{t} \end{bmatrix}_{z_{j+1}} \tag{23}$$

where $h_j = z_{j+1} - z_j$ is again the thickness of layer j.

Therefore, we can finally express the displacement $\boldsymbol{u}$ and traction $\boldsymbol{t}$ on the upper interface by those on the lower interface of layer j as

$$\begin{bmatrix} \boldsymbol{u} \\ \boldsymbol{t} \end{bmatrix}_{z_{j+1}} = \begin{bmatrix} \boldsymbol{A}_1\langle \mathrm{e}^{s^*h_j}\rangle & \boldsymbol{A}_2\langle \mathrm{e}^{-s^*h_j}\rangle \\ \boldsymbol{B}_1\langle \mathrm{e}^{(s^*+\eta)h_j}\rangle & \boldsymbol{B}_2\langle \mathrm{e}^{(-s^*+\eta)h_j}\rangle \end{bmatrix}_j \begin{bmatrix} \boldsymbol{A}_1 & \boldsymbol{A}_2 \\ \boldsymbol{B}_1 & \boldsymbol{B}_2 \end{bmatrix}_j^{-1} \begin{bmatrix} \boldsymbol{u} \\ \boldsymbol{t} \end{bmatrix}_{z_j} \tag{24}$$

Table 1
Material coefficients of the piezoelectric $BaTiO_3$ (C_{ij}^0 in 10^9 N/m^2, e_{ij}^0 in C/m^2, ε_{ij}^0 in 10^{-9} C^2/(N m^2), and μ_{ij}^0 in 10^{-6} N s^2/C^2)

$C_{11}^0 = C_{22}^0$	C_{12}^0	$C_{13}^0 = C_{23}^0$	C_{33}^0	$C_{44}^0 = C_{55}^0$	$C_{66}^0 = 0.5(C_{11}^0 - C_{12}^0)$
166	77	78	162	43	44.5
$e_{31}^0 = e_{32}^0$	e_{33}^0	$e_{24}^0 = e_{15}^0$			
−4.4	18.6	11.6			
$\varepsilon_{11}^0 = \varepsilon_{22}^0$	ε_{33}^0		$\mu_{11}^0 = \mu_{22}^0$	μ_{33}^0	
11.2	12.6		5	10	

Assuming that the displacement $\boldsymbol{u}$ and traction $\boldsymbol{t}$ are continuous across the interfaces, Eq. (24) can be applied repeatedly so that one can propagate the physical quantities from the bottom surface $z = 0$ to the top surface $z = H$ of the multilayered FGM plate. Consequently, we have

$$\begin{bmatrix} \boldsymbol{u} \\ \boldsymbol{t} \end{bmatrix}_H = P_N(h_N)P_{N-1}(h_{N-1})\cdots P_2(h_2)P_1(h_1)\begin{bmatrix} \boldsymbol{u} \\ \boldsymbol{t} \end{bmatrix}_0 \tag{25}$$

Table 2
Material coefficients of the magnetostrictive $CoFe_2O_4$ (C_{ij}^0 in 10^9 N/m^2, q_{ij}^0 in N/(Am), ε_{ij}^0 in 10^{-9} C^2/(N m^2), and μ_{ij}^0 in 10^{-6} N s^2/C^2)

$C_{11}^0 = C_{22}^0$	C_{12}^0	$C_{13}^0 = C_{23}^0$	C_{33}^0	$C_{44}^0 = C_{55}^0$	$C_{66}^0 = 0.5(C_{11}^0 - C_{12}^0)$
286	173	170.5	269.5	45.3	56.5
$q_{31}^0 = q_{32}^0$	q_{33}^0	$q_{24}^0 = q_{15}^0$			
580.3	699.7	550			
$\varepsilon_{11}^0 = \varepsilon_{22}^0$	ε_{33}^0		$\mu_{11}^0 = \mu_{22}^0$	μ_{33}^0	
0.08	0.093		−590	157	

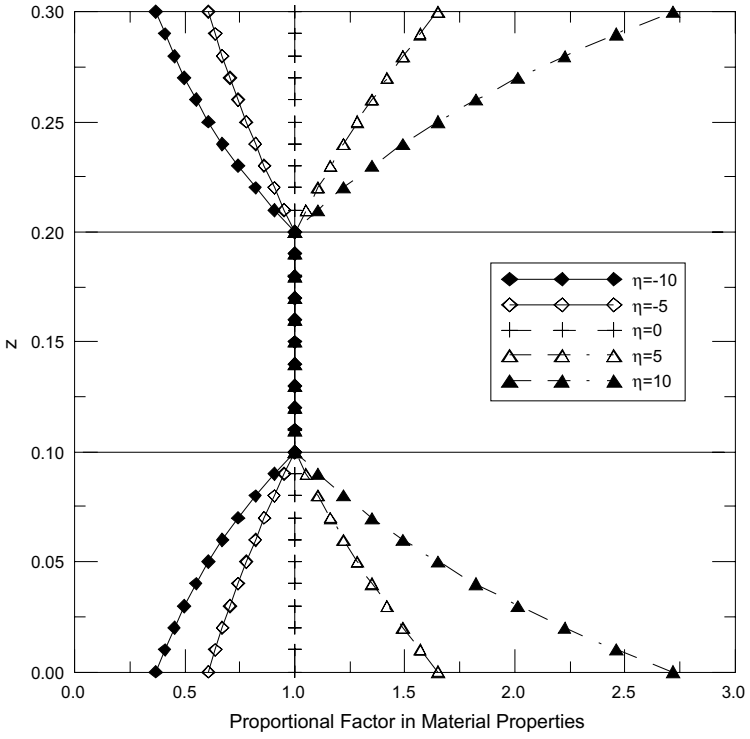

Fig. 1. Variation of the FGM proportional coefficient for $\eta = -10, -5, 0, 5, 10$ (z in m and η in m^{-1}). For $z \in [0.2, 0.3]$, the coefficient is the exponential factor $e^{\eta(z-0.2)}$. The proportional coefficient in $z \in [0, 0.1]$ is obtained via symmetric requirement.

where

$$P_k(h_k) = \begin{bmatrix} \boldsymbol{A}_1\langle e^{s^* h_k}\rangle & \boldsymbol{A}_2\langle e^{-s^* h_k}\rangle \\ \boldsymbol{B}_1\langle e^{(s^*+\eta)h_k}\rangle & \boldsymbol{B}_2\langle e^{(-s^*+\eta)h_k}\rangle \end{bmatrix}_k \begin{bmatrix} \boldsymbol{A}_1 & \boldsymbol{A}_2 \\ \boldsymbol{B}_1 & \boldsymbol{B}_2 \end{bmatrix}_k^{-1} \quad (k = 1, \ldots, N) \tag{26}$$

is called the propagating matrix or propagator.

Eq. (25) is a surprisingly simple relation, and for given boundary conditions, can be solved for the unknowns involved. As examples, the mechanical and electric loads will be discussed.

In the first example, we assume that, on the top surface ($z = H$) the z-direction traction component is applied, i.e.,

$$\sigma_{zz} = \sigma_0 \sin px \sin qy \tag{27}$$

which may represent one of the terms in the double Fourier series solution for a general loading case (uniform or point loading). All other traction components on both surfaces are assumed to be zero. Thus, Eq. (25) is reduced to

$$\begin{bmatrix} \boldsymbol{u} \\ \boldsymbol{t} \end{bmatrix}_H = \begin{bmatrix} \boldsymbol{M}_1 & \boldsymbol{M}_2 \\ \boldsymbol{M}_3 & \boldsymbol{M}_4 \end{bmatrix} \begin{bmatrix} \boldsymbol{u} \\ \boldsymbol{0} \end{bmatrix}_0 \tag{28}$$

where the four submatrices $\boldsymbol{M}_j$ are the multiplications of the propagator matrices in Eq. (25).

Applying the traction boundary condition (27), the left-hand side of Eq. (28) on the top surface is expressed as

$$\begin{bmatrix} \boldsymbol{u} \\ \boldsymbol{t} \end{bmatrix}_H = [u_x, u_y, u_z, \phi, \psi, 0, 0, \sigma_0 \sin px \sin qy, 0, 0]^{\mathrm{t}} \tag{29}$$

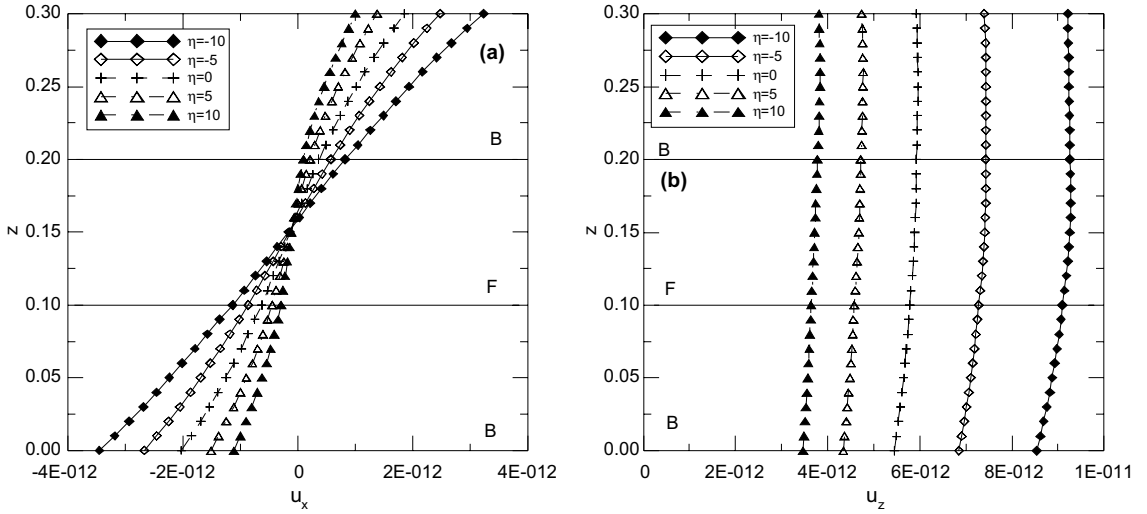

Fig. 2. Variation of the elastic displacement components u_x and u_z (m) along the thickness direction in FGM magneto-electro-elastic B/F/B for factor $\eta = -10, -5, 0, 5, 10$ (m^{-1}) caused by a surface load on the top surface. u_x in (a) and u_z in (b).

The unknown extended displacements on both surfaces of the multilayered FGM plate can thus be solved from Eq. (28).

In the second example, the traction vector $\boldsymbol{t}$ on the bottom surface is again assumed to be zero, but we apply an electric potential ϕ to the top surface ($z = H$), given as,

$$\phi = \phi_0 \sin px \sin qy \tag{30}$$

For this case, the left-hand side of Eq. (28), i.e. the boundary values on the top surface, becomes

$$\begin{bmatrix} \boldsymbol{u} \\ \boldsymbol{t} \end{bmatrix}_H = [u_x, u_y, u_z, \phi_0 \sin px \sin qy, \psi, 0, 0, 0, D_z, 0]^{\mathrm{t}} \tag{31}$$

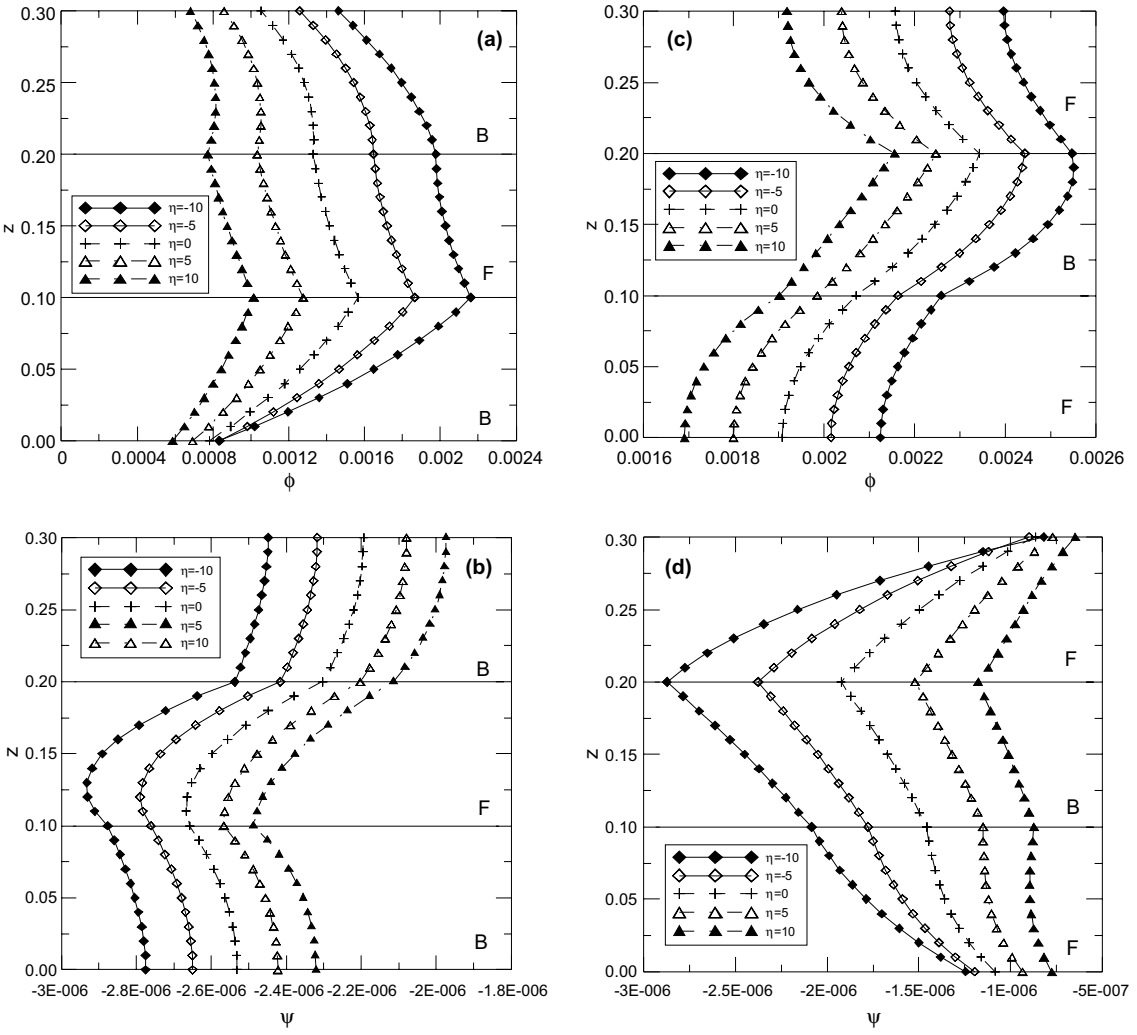

Fig. 3. Variation of electric potential ϕ (V) and magnetic potential ψ (C/s) along the thickness direction in FGM magneto-electro-elastic plates for factor $\eta = -10, -5, 0, 5, 10$ (m^{-1}) caused by a surface load on the top surface. ϕ in (a) and ψ in (b) for B/F/B, and ϕ in (c) and ψ in (d) for F/B/F.

Following the same procedures, all the unknowns on the top and bottom surfaces can be found from Eq. (28).

In order to obtain the extended displacement and traction vectors at any depth, say $z_k \leqslant z \leqslant z_{k+1}$ in layer k, we propagate the solution from the bottom of the layered plate to the z-level, i.e.,

$$\begin{bmatrix} \boldsymbol{u} \\ \boldsymbol{t} \end{bmatrix}_z = \boldsymbol{P}_z(z - z_{k-1})\boldsymbol{P}_{k-1}(h_{k-1}) \cdots \boldsymbol{P}_2(h_2)\boldsymbol{P}_1(h_1) \begin{bmatrix} \boldsymbol{u} \\ \boldsymbol{t} \end{bmatrix}_0 \tag{32}$$

With the extended displacement and traction vectors at a given depth being solved, the corresponding in-plane quantities can be evaluated using Eqs. (16) and (17).

Similar solutions can also be obtained for other boundary conditions. Therefore, for an anisotropic, magneto-electro-elastic, and FGM multilayered rectangular plate, we have derived the exact solution based on the pseudo-Stroh formalism and the propagator matrix method. In the next section, we apply our solution to investigate the response of the sandwiched FGM plate under mechanical and electric loads.

5. Numerical analyses

In the numerical calculation, the layered FGM plate is made of three layers. The z-independent material coefficients are piezoelectric $BaTiO_3$ and magnetostrictive $CoFe_2O_4$, listed respectively, in Tables 1 and 2 [4]. It is obvious that the piezoelectric $BaTiO_3$ and magnetostrictive $CoFe_2O_4$ are both transversely isotropic with their symmetry axis along the z-axis. The three layers have equal thickness of 0.1 m (with a total thickness $H = 0.3$ m) and the horizontal dimensions of the plate are $L_x \times L_y = 1\ \text{m} \times 1\ \text{m}$. Two sandwich plates with stacking sequences $BaTiO_3/CoFe_2O_4/BaTiO_3$

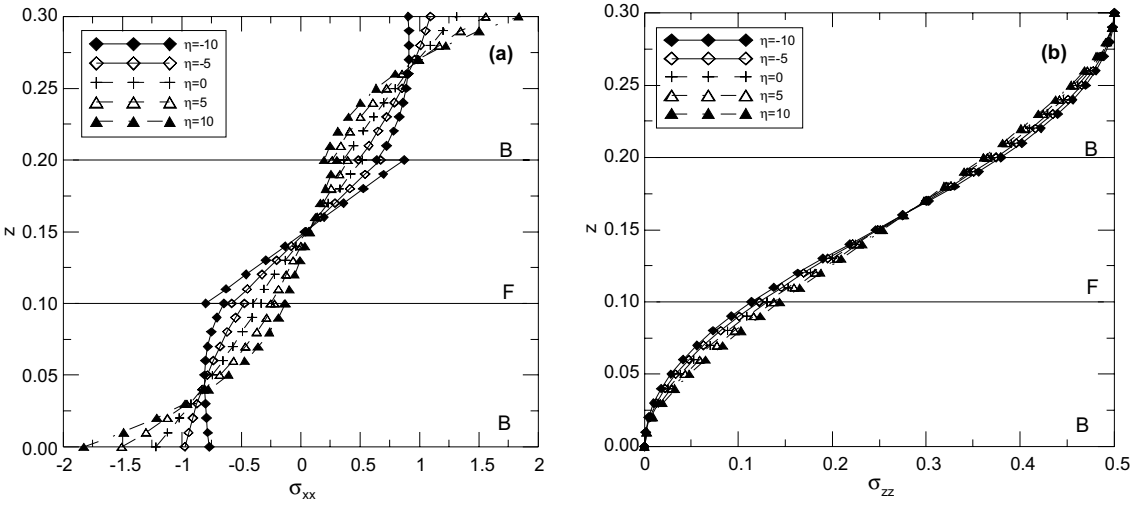

Fig. 4. Variation of stress components σ_{xx} and σ_{zz} (N/m^2) along the thickness direction in FGM magneto-electro-elastic B/F/B plate for factor $\eta = -10, -5, 0, 5, 10$ (m^{-1}) caused by a surface load on the top surface. σ_{xx} in (a) and σ_{zz} in (b).

(called B/F/B) and $CoFe_2O_4/BaTiO_3/CoFe_2O_4$ (called F/B/F) are investigated. While the middle layer is homogeneous, both the top and bottom layers are functionally graded with the symmetric exponential variation shown in Fig. 1. As can also be observed from Fig. 1, five different exponential factors, i.e., $\eta = -10, -5, 0, 5, 10$ (m^{-1}), were studied.

For both the mechanical and electric loadings, the investigated mode is fixed at $m = n = 1$ (i.e., $p = \pi/L_x$, $q = \pi/L_y$ in Eqs. (27) and (30)) and the horizontal coordinates are fixed at $(x, y) = (0.75L_x, 0.25L_y)$. The amplitudes in Eqs. (27) and (30) are, respectively, $\sigma_0 = 1$ N/m^2 and $\phi_0 = 1$ V. It has been checked that under the mechanical load, the results corresponding to the exponential factor $\eta = 0$ are exactly the same as those in Pan [4].

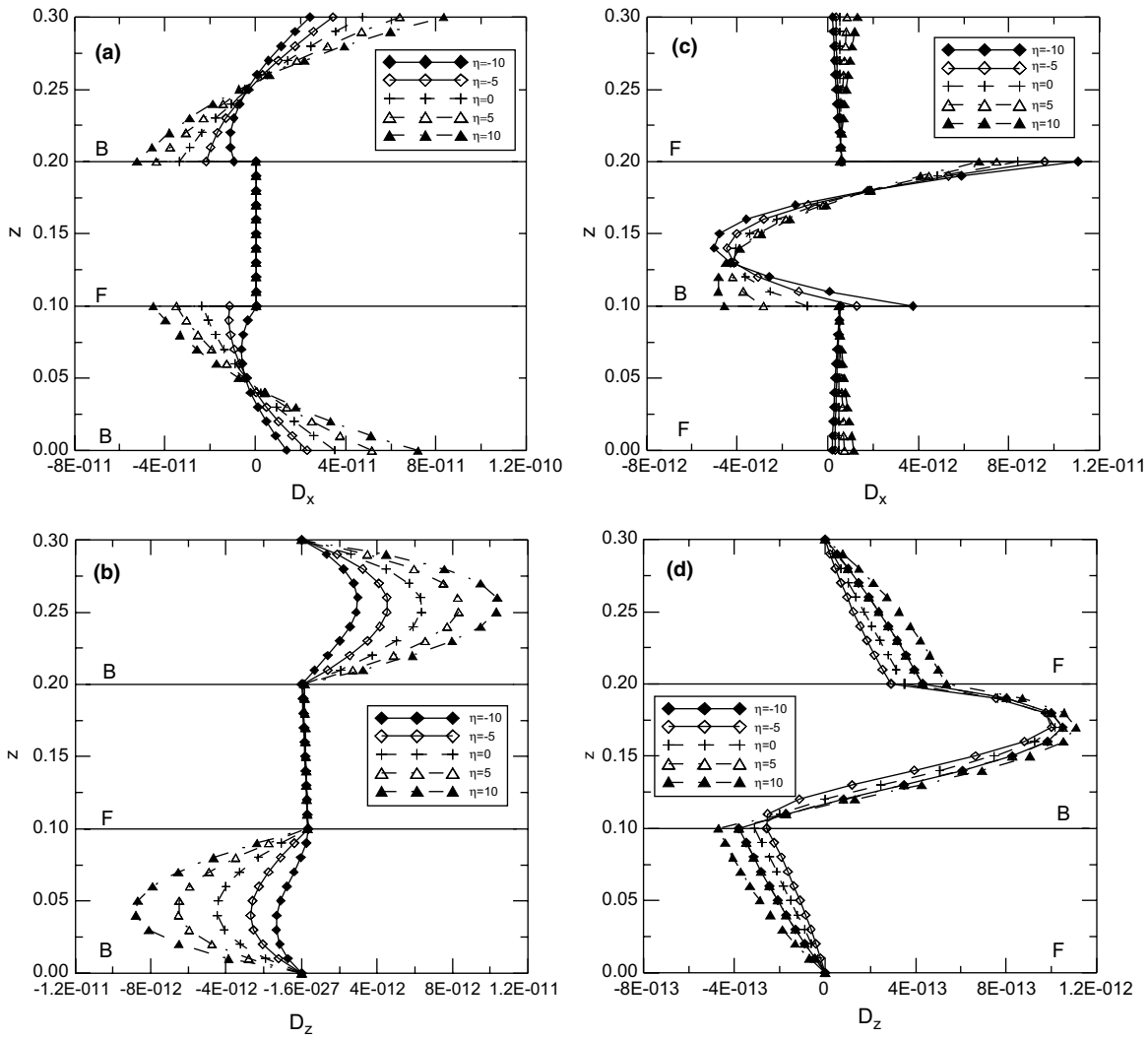

Fig. 5. Variation of electric displacement components D_x and D_z (C/m^2) along the thickness direction in FGM magneto-electro-elastic plates for factor $\eta = -10, -5, 0, 5, 10$ (m^{-1}) caused by a surface load on the top surface. D_x in (a) and D_z in (b) for the B/F/B case, and D_x in (c) and D_z in (d) for the F/B/F case.

5.1. Mechanical load

Fig. 2a and b shows, respectively, the variation of the elastic displacements u_x ($=-u_y$) and u_z along the z-direction in the FGM B/F/B plate. Variation of these elastic displacements in the corresponding F/B/F plate is similar to those in Fig. 2a and b, with only slight difference in the magnitude (magnitude of the elastic displacement in B/F/B is generally larger than that in F/B/F). It is observed that on the top and bottom surfaces, the magnitude of the horizontal displacement u_x increases with decreasing exponential factor η. Furthermore, on the top surface the horizontal

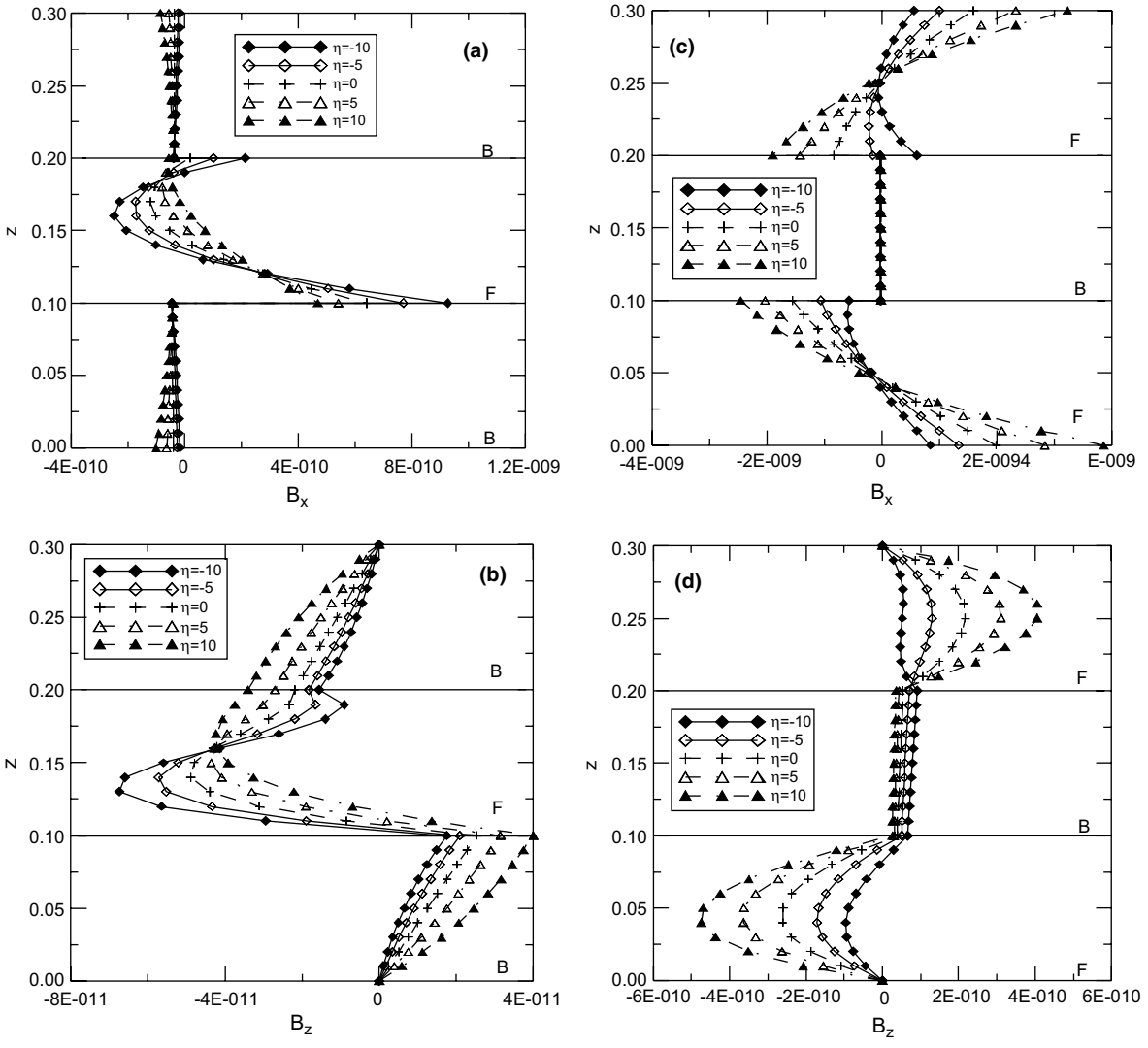

Fig. 6. Variation of magnetic induction components B_x and B_z (Wb/m^2) along the thickness direction in FGM magneto-electro-elastic plates for factor $\eta = -10, -5, 0, 5, 10$ (m^{-1}) caused by a surface load on the top surface. B_x in (a) and B_z in (b) for the B/F/B case, and B_x in (c) and B_z in (d) for the F/B/F case.

displacement is positive, while on the bottom surface they are negative. As for the vertical displacement u_z, its value increases with decreasing η in the whole plate.

Fig. 3a and b shows, respectively, the variation of the electric potential ϕ and magnetic potential ψ along the z-direction in the B/F/B plate. The results in the corresponding F/B/F plate are plotted in Fig. 3c and d. It is observed that in both plate models, the magnitudes of the electric and magnetic potentials decreases with increasing factor η. It is further noticed that even though these potentials are continuous across the interfaces, their slopes are not (i.e., Fig. 3a at $z = 0.1$ m, and Fig. 3d at $z = 0.2$ m).

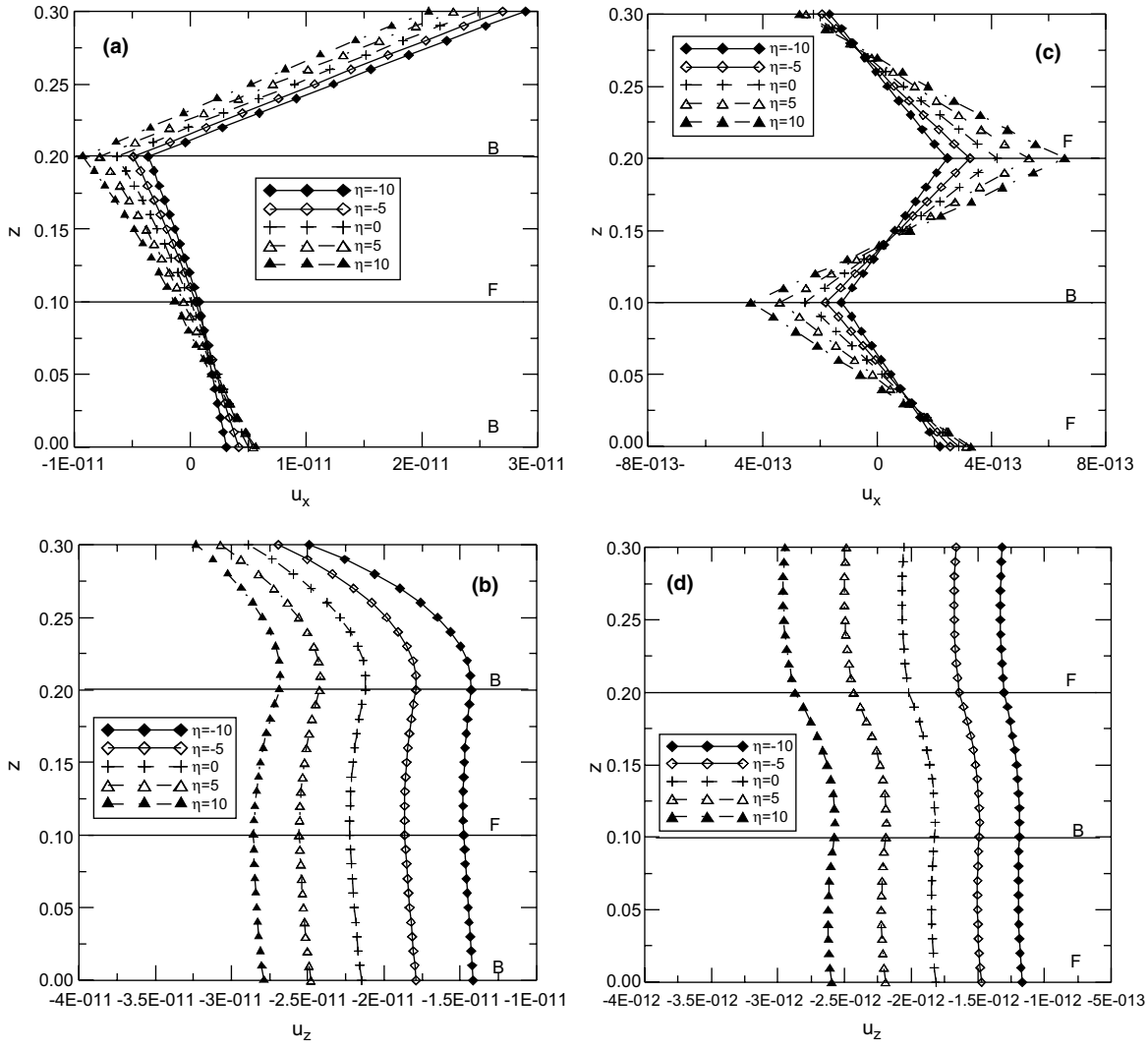

Fig. 7. Variation of the elastic displacement components u_x and u_z (m) along the thickness direction in FGM magneto-electro-elastic plates for factor $\eta = -10, -5, 0, 5, 10$ (m^{-1}) caused by an electric potential on the top surface. u_x in (a) and u_z in (b) for the B/F/B case, and u_x in (c) and u_z in (d) for the F/B/F case.

Fig. 4a and b shows, respectively, the variation of the stress components σ_{xx} (=σ_{yy}) and σ_{zz} along the z-direction for the B/F/B plate. The results in the corresponding F/B/F plate are very similar to those shown in Fig. 4a and b (for both curve shapes and magnitudes). While the normal stress σ_{zz} does not change much for different factor η (Fig. 4b), the horizontal normal stress σ_{xx} is very sensitive to the exponential factor η. Near the interfaces or surfaces (Fig. 4a), its magnitude can be doubled by varying η from -10 to 10 (m^{-1}). Furthermore, the horizontal stress component is discontinuous across the interface, as expected.

The variations of the electric displacements D_x (=$-D_y$), D_z and magnetic inductions B_x (=$-B_y$), B_z along the z-direction are plotted, respectively, in Figs. 5a–d and 6a–d. While Figs. 5a,b and 6a,b are for the B/F/B plate, Figs. 5c,d and 6c,d for the F/B/F plate. It is observed, from these figures, that because of the material property discontinuities in different layers, the horizontal electric displacement and magnetic induction are discontinuous across the interfaces. It is also interesting to note that the magnitude of horizontal electric displacement (magnetic induction) is very small in magnetostrictive $CoFe_2O_4$ (piezoelectric $BaTiO_3$) layers, due to the fact that for magnetostrictive $CoFe_2O_4$ (piezoelectric $BaTiO_3$) material, the piezoelectric (piezomagnetic) coefficients are zero. Furthermore, the similarity among the response curves should be also noticed: D_x in Fig. 5a vs. B_x in Fig. 6c; D_z in Fig. 5b vs. B_z in Fig. 6d; D_x in Fig. 5c vs. B_x in Fig. 6a; and D_z in Fig. 5d vs. B_z in Fig. 6b.

5.2. Electric load

Fig. 7a and b shows, respectively, the variations of the elastic displacements u_x (=$-u_y$) and u_z along the z-direction for the B/F/B plate, whilst Fig. 7c and d is the corresponding elastic displacements for the F/B/F plate. In contrast to the mechanical load case, we observe here clearly that the

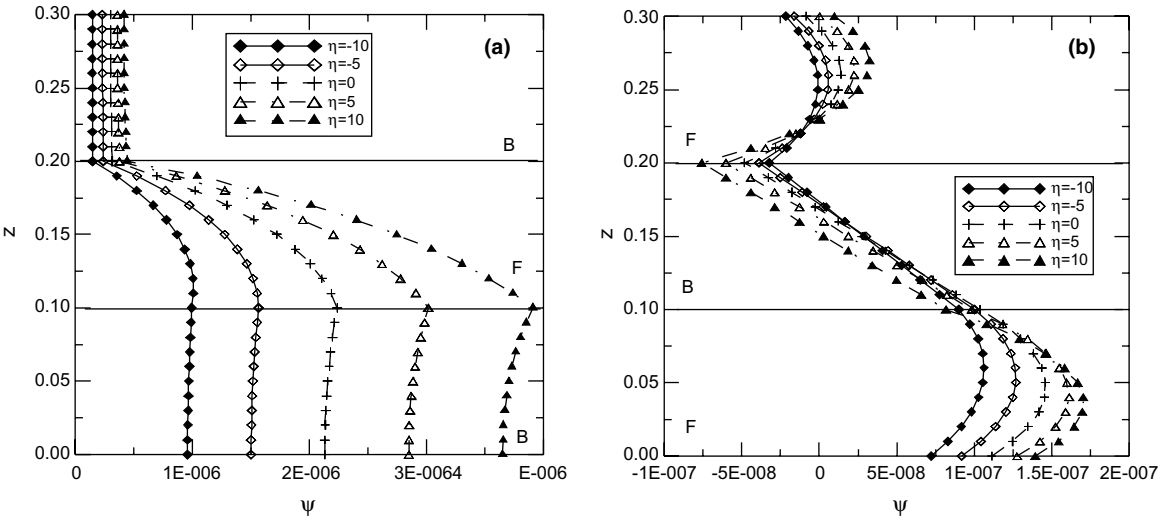

Fig. 8. Variation of magnetic potential ψ (C/s) along the thickness direction in FGM magneto-electro-elastic plates for factor $\eta = -10, -5, 0, 5, 10$ (m^{-1}) caused by an electric potential on the top surface. ψ in (a) for the B/F/B case and ψ in (b) for the F/B/F case.

elastic displacements in the two sandwich plates are completely different from each other. In particular, the magnitude of the elastic displacements in B/F/B is roughly one order larger than that in F/B/F.

The magnetic potential ψ along the z-direction in the B/F/B and F/B/F plates are shown, respectively, in Fig. 8a and b. It is interesting that for both sandwich plates, relatively large magnetic potential can be induced in the bottom layer when an electric potential is applied on the top surface. Furthermore, in the bottom layer, the magnitude of the magnetic potential in B/F/B is larger than that in F/B/F.

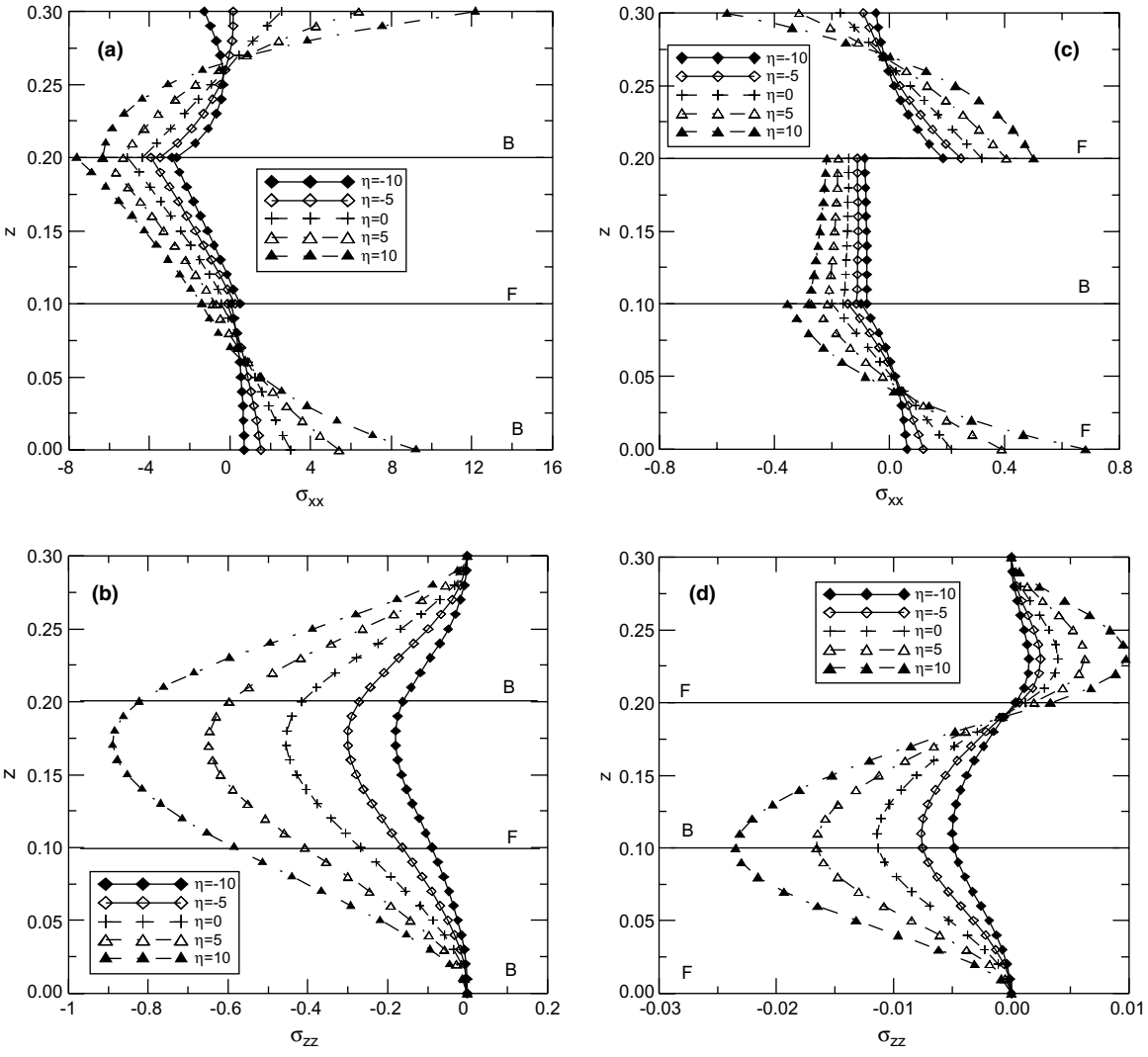

Fig. 9. Variation of stress components σ_{xx} and σ_{zz} (N/m^2) along the thickness direction in FGM magneto-electro-elastic plates for factor $\eta = -10, -5, 0, 5, 10$ (m^{-1}) caused by an electric potential on the top surface. σ_{xx} in (a) and σ_{zz} in (b) for the B/F/B case, and σ_{xx} in (c) and σ_{zz} in (d) for the F/B/F case.

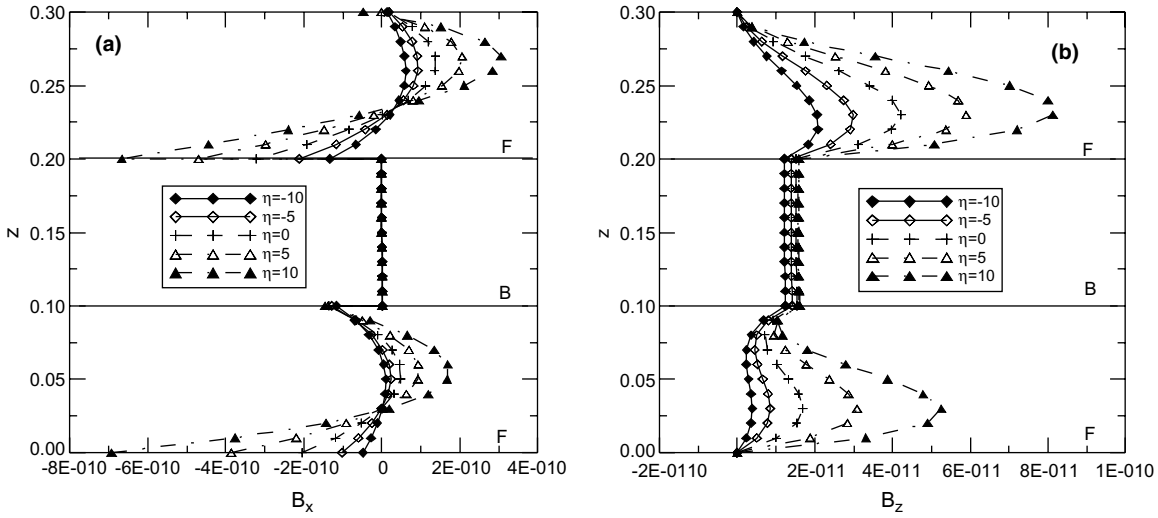

Fig. 10. Variation of magnetic induction components B_x and B_z (Wb/m^2) along the thickness direction in FGM magneto-electro-elastic F/B/F for factor $\eta = -10, -5, 0, 5, 10$ (m^{-1}) caused by an electric potential on the top surface. B_x in (a) and B_z in (b).

Fig. 9a and b shows, respectively, the variation of the stress components σ_{xx} ($=\sigma_{yy}$) and σ_{zz} along the z-direction for the B/F/B plate. The results for the corresponding F/B/F plate are plotted in Fig. 9c and d. In contrast to the mechanical load (Fig. 4a and b); the stacking sequence now has a dramatic influence on the stress components in terms of both the curve shape and magnitude (Fig. 9a vs. Fig. 9c and Fig. 9b vs. Fig. 9d). Furthermore, the normal stress component σ_{zz} can be greatly altered by varying the exponential factor η (Fig. 9b and d), as compared to the mechanical loading case.

Finally, Fig. 10a and b shows, respectively, the variations of magnetic inductions B_x ($=-B_y$), B_z along the z-direction in F/B/F case. It is observed that the magnetic induction changes dramatically in the top and bottom layers (magnetostrictive $CoFe_2O_4$), and it is almost zero in the middle layer (piezoelectric $BaTiO_3$). In other words, relatively large magnetic field can still be induced in the magnetostrictive layer even if an electric load is applied.

6. Conclusions

In this paper, an exact solution is presented for a layered rectangular plate made of anisotropic and functionally graded magneto-electro-elastic materials. The plate is under simply supported edge conditions and both the mechanical and electric loads are applied on the top surface of the plate. While the homogeneous solution in each FGM layer is derived based on the pseudo-Stroh formalism, the propagator matrix method is employed to handle the multilayered structures. In the numerical study, two sandwich plates are analyzed, which are made of piezoelectric $BaTiO_3$ and magnetostrictive $CoFe_2O_4$, with material properties varying exponentially in the thickness direction within the top and bottom layers. It is observed that, in general, different

exponential factors will produce different magnitudes for the response curves. Furthermore, the stacking sequences (B/F/B or F/B/F) and the boundary conditions (mechanical or electric load) can have significant effects on the induced magnetic, electric, and elastic fields. An interesting example is that, under the mechanical load, the normal stress component σ_{zz} is very insensitive to the exponential factor; however, under the electric potential, different exponential factors can produce completely different normal stress components. While the numerical examples can serve as benchmarks for various numerical methods, the special characteristics discussed in this paper should be useful to the design of smart structures based on the piezoelectric and magnetostrictive FGMs.

References

[1] G. Harshe, J.P. Dougherty, R.E. Newnham, Theoretical modeling of multiplayer magnetoelectric composites, Int. J. Appl. Electromagn. Mater. 4 (1993) 145–159.
[2] C.W. Nan, Magnetoelectric effect in composites of piezoelectric and piezomagnetic phases, Phys. Rev. B 50 (1994) 6082–6088.
[3] Y. Benveniste, Magnetoelectric effect in fibrous composites with piezoelectric and piezomagnetic phases, Phys. Rev. B 51 (1995) 16424–16427.
[4] E. Pan, Exact solution for simply supported and multilayered magneto-electro-elastic plates, J. Appl. Mech. 68 (2001) 608–618.
[5] E. Pan, P. Heyliger, Free vibrations of simply supported and multilayered magneto-electro-elastic plates, J. Sound Vib. 253 (2002) 429–443.
[6] J. Li, M.L. Dunn, Micromechanics of magnetoelectroelastic composite materials: average fields and effective behavior, J. Intel. Mater. Sys. Struct. 9 (1998) 404–416.
[7] X. Wang, Y. Shen, Inclusions of arbitrary shape in magnetoelectroelastic composite materials, Int. J. Eng. Sci. 41 (2003) 85–102.
[8] C. Gao, H. Kessler, H. Balke, Crack problems in magnetoelectroelastic solids, Part I: exact solution of crack, Int. J. Eng. Sci. 41 (2003) 969–981.
[9] X.Q. He, T.Y. Ng, S. Sivashanker, K.M. Liew, Active control of FGM plates with integrated piezoelectric sensors and actuators, Int. J. Eng. Sci. 38 (2001) 1641–1655.
[10] K.M. Liew, J. Yang, S. Kitipronchai, Postbuckling of piezoelectric FGM plates subject to thermo-electro-mechanical loading, Int. J. Solids Struct. 40 (2003) 3869–3892.
[11] Y.Y. Yang, Time-dependent stress analysis in functionally graded materials, Int. J. Solids Struct. 37 (2000) 7593–7608.
[12] J. Xu, X. Zhu, Z. Meng, Effect of the interdiffusion reaction on the compatibility in PZT/PNN functionally gradient piezoelectric materials, IEEE Trans. Compon. Packag. Technol. 22 (1999) 11–16.
[13] A.A. Almajid, M. Taya, 2D-elasticity of FGM piezo-laminates under cylindrical bending, J. Intel. Mater. Syst. Struct. 12 (2001) 341–351.
[14] A.A. Almajid, M. Taya, S. Hudnut, Analysis of out-of-plane displacement and stress field in a piezocomposite plate with functinonally graded microstructure, Int. J. Solids Struct. 38 (2000) 3377–3391.
[15] E. Pan, Exact solution for functionally graded anisotropic elastic composite laminates, J. Compos. Mater. 37 (2003) 1903–1920.
[16] Z. Zhong, E.T. Shang, Three-dimensional exact analysis of a simply supported functionally gradient piezoelectric plate, Int. J. Solids Struct. 40 (2003) 5335–5352.
[17] A.N. Stroh, Dislocations and cracks in anisotropic elasticity, Philos. Mag. 3 (1958) 625–646.
[18] T.C.T. Ting, Anisotropic Elasticity, Oxford University Press, Oxford, 1996.
[19] T.C.T. Ting, Recent developments in anisotropic elasticity, Int. J. Solids Struct. 37 (2000) 401–409.
[20] F. Gilbert, G. Backus, Propagator matrices in elastic wave and vibration problems, Geophysics 31 (1966) 326–332.

[21] E. Pan, A general boundary element analysis of 2-D linear elastic fracture mechanics, Int. J. Fract. 88 (1997) 41–59.
[22] E. Pan, Static Green's functions in multilayered half spaces, Appl. Math. Modelling 21 (1997) 509–521.
[23] S.K. Datta, Wave propagation in composite plates and shells, in: Comprehensive Composite Materials, Elsevier, New York, 2000, pp. 511–558.
[24] E. Pan, An exact solution for transversely isotropic, simply supported and layered rectangular plates, J. Elast. 25 (1991) 101–116.
[25] P. Bisegna, F. Maceri, An exact three-dimensional solution for simply supported rectangular piezoelectric plates, J. Appl. Mech. 63 (1996) 628–638.
[26] N.J. Pagano, Exact solutions for rectangular bidirectional composites and sandwich plates, J. Compos. Mater. 4 (1970) 20–34.
[27] P. Heyliger, Exact solutions for simply supported laminated piezoelectric plates, J. Appl. Mech. 64 (1997) 299–306.